Case Studies in Construction Materials 17 (2022) e01370

Contents lists available at ScienceDirect

Case Studies in Construction Materials

journal homepage: www.elsevier.com/locate/cscm

Fatigue bond-slip properties of steel reinforcing bars embedded in UHPFRC: Extraction and development of an accumulated damage law

Barbara Daniela Giorgini Sepulveda, Phillip Visintin *, Deric John Oehlers

School of Civil, Environmental and Mining Engineering, The University of Adelaide, North Tce, Adelaide, South Australia 5005, Australia

ARTICLE INFO

Keywords:
Bond
Fatigue
UHPFRC
Incremental set
Bond stiffness

ABSTRACT

The occurrence of cyclic loads in RC structures is known to deteriorate the bond between the reinforcing bars and concrete by reducing both the bond strength and stiffness, eventually leading to debonding through large increases in slip. There is much research to quantify this bond deterioration for normal strength concrete but little research has considered UHPFRC, which is the subject of this paper. This research develops a testing approach and analysis procedure to quantify the deterioration in bond as a result of high-cycle fatigue. The procedure has been developed through 18 tests of steel reinforcing bars embedded in UHPFRC with steel micro fibres. A test rig has been developed to directly measure the bond-slip under monotonic and cyclic loads. Procedures are then developed for quantifying the bond stiffness and the incremental set, that is, the increase in slip per cycle, by using the known interaction between the monotonic and cyclic bond-slip already identified by other researchers. It is shown how these procedures can be used to quantify the bond degradation under combinations of fatigue loads and how simply measuring the crack width in a structure can give a very good indication of both the residual fatigue life and bond strength.

1. Introduction

Bond and the deterioration in bond affect ultimate limit-state behaviour, including strength and ductility through the development of stresses in reinforcement and reinforcement debonding [1,2], and serviceability limit-state behaviour through tension-stiffening and the distribution and width of cracks [3]. Under high-cycle fatigue, experimental testing on concrete has shown that deterioration of bond may occur even under low cyclic stress ranges due to the formation of internal micro cracks and the crushing of concrete in front of reinforcement lugs [4,5], and this deterioration has been shown to lead to a reduction in structural service-life [6–8].

Through testing, many parameters have been found to influence bond-slip behaviour under fatigue loading. These parameters relate to the concrete material properties (mix design, concrete strength, the presence and volume of fibres), the reinforcement properties (bar size, shape and distribution of lugs), environmental conditions (temperature or exposure to harsh environments that may degrade concrete or reinforcement properties), specimen geometry (concrete cover) and the loading condition (frequency, range and magnitude of the cyclic stress) [9–23].

While the above references show that the parametric variation in bond behaviour under fatigue loading has been broadly

* Corresponding author.
E-mail address: phillip.visintin@adelaide.edu.au (P. Visintin).

https://doi.org/10.1016/j.cscm.2022.e01370
Received 30 May 2022; Received in revised form 18 July 2022; Accepted 1 August 2022
Available online 2 August 2022

Nomenclature

b	Exponent of fatigue equation of slip
CF	Cycled to failure test
CL	Confidence limit
D	Fatigue damage
D_{stb}	Fatigue damage in stable region
D_{unstb}	Fatigue damage in unstable region
f	Frequency
f_k	kth level of frequency
f_c	Concrete cylinder strength
k	Cyclic stiffness; cyclic range of stress divided by slip between peak and trough
k_{po}	k at onset of pullout
k_{st}	k at start of cyclic loading
k_{stb}	k at end of stable region
LF	Loaded to failure test
N	Number of cycles of load
N_{blk}	Any block of N cycles
N_p	Number of cycles at half N_{stb}
N_{po}	N at pullout failure
N_{tran}	N to first stabilise β
N_{stb}	N at the end of the stable region β_{stb}
N_t	total number of cycles applied in a test
P	τ_{pk}/τ_{max}
R	τ_r/τ_{max}
RC	Reinforced concrete
S	Bond slip
S_N	total slip
SD	Standard deviation
T	τ_{tr}/τ_{max}
S_{asc}	S at the peak of the monotonic ascending branch
S_{max}	S at τ_{max}; S at end of bond ductile plate at τ_{max}
S_N	Total slip
S_p	Slip at N_p that corresponds to the slip at half ΔS_{stb}
S_{pk}	S at the peak of first cyclic loading
S_{po}	S at onset of pullout failure
S_{rs}	S at the maximum residual strength
S_{st}	S at start of cyclic loading
UHPFRC	Ultra high performance fibre reinforced concrete
z	Number of cyclic ranges
β	Incremental set; increase in slip in a cycle of load
β_{stb}	Stable incremental set
$\beta_{stb\text{-}k}$	kth level of stable incremental
β_{tran}	Average incremental set in initial transition zone
β_{unstb}	Average unstable incremental set
$\beta_{unstb\text{-}k}$	kth level of unstable incremental
ΔS_{stb}	Increase in slip over stable region
$\Delta S_{stb\text{-}fat}$	Increase in slip whilst in stable region in fatigue analysis
ΔS_{tran}	Increase in slip over initial transition zone
ΔS_{unstb}	Increase in slip over unstable stable region
τ	Bond shear stress
τ_{max}	Maximum monotonic shear strength
τ_{pk}	τ at peak of cyclic load
τ_{tr}	τ at trough of cyclic load
τ_r	Cyclic range of shear stress
τ_{rs}	Residual shear strength

investigated for normal strength concretes without fibres, to date, there is very little test data available for ultra-high performance fibre reinforced concrete (UHPFRC). This is particularly important because UHPFRC is widely promoted on the basis of its ability to minimise serviceability deflections and crack widths, but this outcome is highly dependent on the bond properties being maintained through a high number of cycles. While several models have been developed to quantify monotonic bond-slip behaviour [24,25], comparatively little is known of the bond under high-cycle fatigue loading. For example, Koschemann et al. [26] tested 9 specimens under high-cycle fatigue with peak bond stresses of between 75% and 80% of the maximum bond stress and showed that UHPFRC pull-out specimens could stand more than 5 million cycles without failure. While an essential first step in developing a high-cycle fatigue bond model, it is now necessary to consider behaviour under a wider range of peak stresses and stress ranges in order to develop a more generic model.

Given Considering that, and given the lack of testing of UHPFRC bond under high-cycle fatigue, the first aim of the paper is to develop experimental data to help quantify the fatigue endurance of UHPFRC.

Now let us consider existing approaches taken to modelling the impact of high-cycle fatigue on bond and the corresponding failure criteria. To allow for the development of analysis procedures, Balazs [27] presented a bond fatigue failure criteria to determine the interaction between the monotonic and fatigue behaviour. In this work, it was concluded that the end of stable crack growth under high cycle fatigue coincided with the slip s_{max} at which the maximum bond stress τ_{max} is reached and, on this basis, it was suggested taking the fatigue failure criteria for design as this point.

Koch and Balázs [28] showed that the lower the cyclic peak $\tau_{pk,}$ the slower the rate of pull out. However, in the tests used to make this conclusion, the range of shear stress τ_r varied directly with the shear stress at the cyclic peak τ_{pk} so that either or both parameters could have affected the rate of pull out. Lin et al. [8] and Oh and Kim [29] further observed that the rate of increase in slip, defined here as the incremental set, was not influenced by the cyclic loading despite the use of different cyclic peaks. These fatigue analyses were however done using test results with a limited number of cycles and for low τ_{pk} and consequently low τ_r, the tests were also terminated before the slip reached S_{max}. As a consequence, no substantial increase in slip was observed. While this approach is justifiable on the basis of the time taken to complete high-cycle fatigue tests, a small number of tests with cycles to failure is required to justify modelling assumptions. In most tests performed, a minimum cyclic load τ_{tr} as a proportion of τ_{max} was maintained, and the range ($R = \tau_r/\tau_{max}$) varied [4,8,14,28,29]. Consequently, the peak ($P = \tau_{pk}/\tau_{max}$) also varied, so these tests are unable to distinguish between the individual effects of the peak stress and range stress. Based on this system of loading, the conclusion drawn was that the peak was the major factor to influence the life of bond although in reality it was likely also the range. No study was found that applied the same peak to different ranges to confirm the influence of the range on the fatigue test. To address the uncertainty regarding the importance of both τ_r/τ_{max} and τ_{pk}/τ_{max} in this paper we design experiments to explicitly consider both τ_r/τ_{max} and τ_{pk}/τ_{max}.

Published research to predict the total slip S_N whilst cycling are summarised in Table 1. All the tests used non-fibre reinforced concrete and their concrete cylinder strengths f_c given in the second column show all have been conducted using normal strength concrete. Also shown in Table 1 are $R = \tau_r/\tau_{max}$ and $P = \tau_{pk}/\tau_{max}$, from which it can be seen that an emphasises has been placed on the importance τ_{max} by researchers. The maximum number of cycles applied (shown in the fifth column) is observed to be relatively small in terms of high cycle fatigue.

All the references in Table 1 except that of Lin et al. [8] used the following form of equation in the analysis of their test results

$$S_N = S_{st}(1+N)^b \tag{1}$$

which was first developed by Rehm and Eligehausen [4].

In Eq. (1), the total slip depends on the initial monotonic slip at the start of cyclic loading S_{st}, the number of cycles applied N and an exponent *b* which is determined empirically and given in the sixth column in Table 1. In four of the studies in Table 1, b is taken as a constant, while in two, it is taken to depend on the peak stress. Hence it can be seen that although the range and peak cyclic stresses are not incorporated directly into Rehm and Eligehausen's Eq. (1), some indirect allowance is made for the peak stresses through their dependence on the b factor, and as the range was directly varied with the peak stress, this equation indirectly allows for the range.

In contrast to Eq. (1), Lin et al. [8] in Table 1 derived the following equation that directly allows for the effect of the peak stress τ_{pk} and as in most tests, the range τ_r was varied with τ_{pk} it allows for the effect of the stress range τ_r.

Table 1
Research on bond fatigue.

References	f_c (MPa)	P (τ_{pk}/τ_{max})	R (τ_r/τ_{max})	Maximum number of cycles applied	Exponent b
Rehm and Eligehausen [4]	24–48 MPa	0.85–0.60	0.75–0.50	10^6	b = 0.107
Koch and Balázs [28]	25 MPa	0.90–0.30	0.27–0.81	2×10^6	b = 0.131 when P < 0.70 τ_{max} b = 0.170 when P < 0.80 τ_{max} average result b= 0.148
Oh and Kim [29]	37 MPa	0.75–0.45	0.75–0.45	10^5	b = 0.098
Zanuy et al. [30,31]	–	–	–	–	b = 0.107 when P < 0.51 τ_{max} $b = 0.447 \bullet P^{2.132}$ when P ≥ 0.51 τ_{max}
Lin et al. [8]	40 MPa	0.75–0.50	0.70 – 0.40	10^5	–
Zhang et al. [14]	38 MPa	0.90–0.65	0.80 – 0.50	1.5×10^6	b = 0.102

$$S_N = S_{max}\left(0.65\frac{\tau_{pk}}{\tau_{max}} + 0.20\right)N^{\left(0.29\frac{\tau_{pk}}{\tau_{max}} - 0.07\right)} \tag{2}$$

From the above research, it can be seen that the number of cycles to reach the total slip S_{max} at which failure occurs N_{stb} is important as this defines the end of the stable region of increase in slip and therefore the fatigue life. Rearranging Eq. (1) to derive the number of cycles N_{stb} when the total slip is S_{max} gives the number of cycles to initiate fatigue damage as

$$N_{stb} = \left(\frac{S_{max}}{S_{st}}\right)^{b^{-1}} - 1 \tag{3}$$

And similarly, rearranging Eq. (2).

$$N_{stb} = \quad S_{max}\left(0.65\frac{\tau_{pk}}{\tau_{max}} - 0.20\right)N^{\left(0.29\frac{\tau_{pk}}{\tau_{max}} - 0.07\right)} \tag{4}$$

Given that the models in Eqs. (1)–(4) and the corresponding calibrations in Table 1 have only been developed for normal strength concrete without fibres, the second major aim of the paper is to develop a fatigue endurance model following the approach of Balazs [27].

In the remainder of the paper, the experimental work to quantify the impact of fatigue on bond between steel reinforcement and UHPFRC is first described, including consideration of the theoretical basis of the test design and specific details of the experimental test performed. This is followed by the presentation of test results, including a description of how to process the measured data to quantify the impact of fatigue range and cyclic peak. It is then shown how the processed test data can be used as the basis for the development of a fatigue endurance model. Finally, a comparison between existing models and those developed here is undertaken.

2. Experimental design

To assist with the design of the experimental work, Fig. 1(a) shows a typical monotonic pull-out test (dashed grey line o-a-d-h-f-g) and a cyclic test (continuous black line o-a-c-e-f-g) so that the two different types (loaded to failure, or cycled to failure) can be defined and their impact on model development assessed. In the monotonic curve, the maximum bond stress τ_{max} occurs at point d at the corresponding slip S_{max}. The cyclic test shown has a constant cyclic peak stress τ_{pk}, trough stress τ_{tr} and range τ_r that is applied during the whole test. At the start of the test, the slip at τ_{pk} is S_{st}. The peak and trough are constant up to point *f* at slip S_{po}, after which the peak τ_{pk} cannot be reached anymore [6] and decreases gradually by following the monotonic envelope along f-g until complete pull out of the reinforcement. In this testing approach, which follows the path o-a-f-g, the specimen is cycled to failure. An alternative testing procedure is to first cycle and then load to failure. For example, the specimen may be cycled from a to c where the slip at *c* is less than S_{max} and then loaded to failure along c-j-d, in which case the peak stress τ_{max} is achieved [29]. In the case where the specimen is cycled to point e (where the slip S_{rs}>S_{max}), then the path follows e-h, and the residual strength at h is τ_{rs} at slip S_{rs} (τ_{rs}< τ_{max}).

Fig. 1(b) shows the change in slip during cyclic loading where the slope or tangent to the line shown as β is the increase in slip per

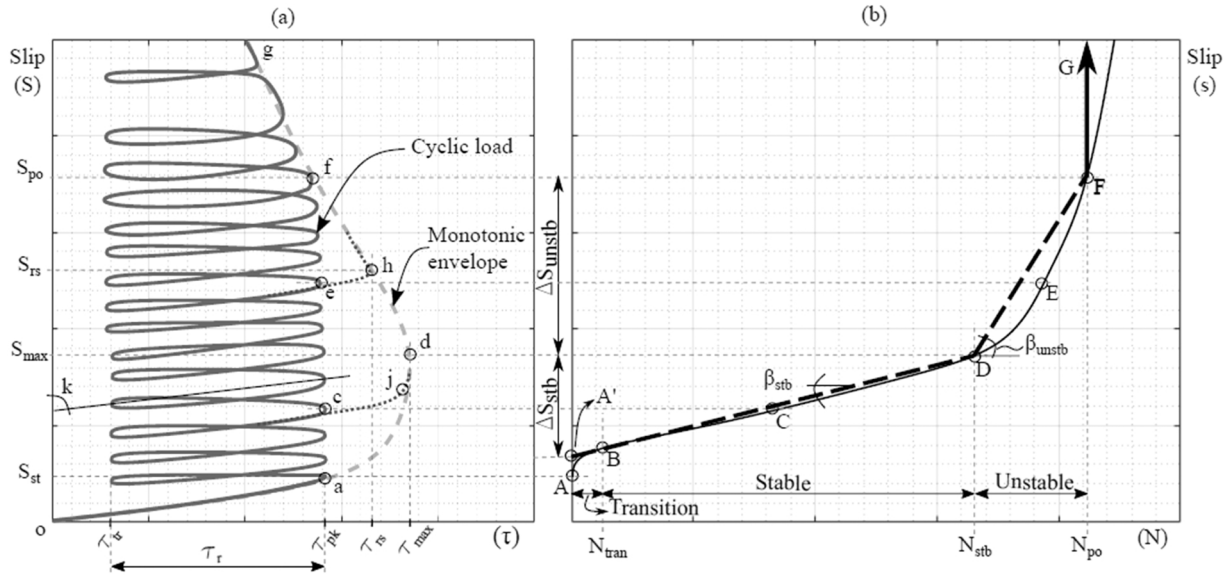

Fig. 1. Interaction between monotonic and cyclic behaviours: (a) Bond-slip; (b) Incremental set.

cycle, that is, the incremental set [4]. For example, at the peak of the first cycle of stress at point a in Fig. 1(a), the total slip is $S_{st,}$ and this is point A in Fig. 1(b). The cyclic stresses in Fig. 1(a) cause the slip at the peak stress to increase along A-B-C-D-E-F-G in Fig. 1(b). From points A to B in Fig. 1(b), which are the initial cycles, the rate of increase in slip (the tangent to the slope β) is first rapid, then diminishes and stabilises at point B [27]. This transition zone is short compared to the subsequent phases. From points B to D, the rate of increase in slip is constant or stable at β_{stb} and this is referred to as the stable region where point D occurs at the slip S_{max} at τ_{max} [27, 29]. From point D to F, β increases rapidly until pull-out at point F where the peak of the cyclic stress τ_{pk} equals the monotonic strength at point f in Fig. 1(a) where the slip is S_{po} [27]. Importantly, in this unstable region, a constant incremental set β_{unstb} can be used to derive the total change in slip in this region.

2.1. Pull-out test specimen and rig

A schematic of the test specimen used in this study is shown in Fig. 2, where the bar is shown to be centrally located with a clear cover of 29.5 mm and which has been shown in testing of the same concrete mix design to be sufficient to avoid splitting under monotonic loading [25]. The bar has a bonded length of two bar diameters to ensure adequate contact surface for extracting the bond-slip properties. This approach ensures that the bond-slip and bond-stress properties do not have a measurable variation within the bonded length, such that the bond-slip relationship is the actual value and not a mean [25,29]. All specimens were manufactured using 16 mm diameter bars, where, as shown in Fig. 3, all specimens had 3 complete ribs and part of a 4th embedded. The reinforcement ribs were measured to be spaced at 8.5 mm and have a height of 0.9 mm, giving a relative rib area of 0.0731. The reinforcement has a yield strength of 535 MPa (0.2% proof strength), ultimate strength of 747 MPa and an elastic modulus of 203 GPa that complies with AS/NZS4671:2019 [32].

The concrete mix design used to manufacture all specimens is identical to that used by Sepulveda et al. [33] to quantify the high-cycle fatigue properties of UHPFRC in direct tension where the concrete has been shown to strain harden in tension. The concrete is batched using sulphate resisting cement, silica fume, mined sand and a high-range water reducing agent with added retarder in a weight ratio according to Table 2. The mortar is reinforced with 13 mm high-strength steel fibres with a diameter of 0.2 mm and an elastic modulus of 42 GPa.

To quantify the monotonic bond stress slip relationship, five specimens were tested. Specimens M1, M2 and M3 were tested at 28 days when the concrete cylinder strength (measured using 100 mm diameter, 200 mm height specimens) was 110 MPa, whereas specimens M4 and M5 were tested at 90 days when the concrete strength was 126 MPa. In addition to these monotonic tests, thirteen specimens in Table 3 were tested under cyclic loading. Seven of the specimens had ranges in one direction, and six had reversed cyclic loads, although the reverse stress was limited to $-0.2\tau_{max}$ to ensure that the direction of slip was not reversed. In selecting the loading regime, not only were different ranges applied but also each range had different peaks and troughs to ensure that the effects of the peak and range could be differentiated. The decision to cover a reversal of stress but not a reversal of slip was made because it has been shown in tension-stiffening tests that it is common for negative bond stresses to occur without a reversal of slip and while significant crack openings remain ([1,30]). By testing a range of different cyclic ranges and peaks it is additionally possible to confirm Balazs' [34] approach to using the monotonic bond stress slip relationship as the failure envelope for bond under high-cycle fatigue. By testing a range of different cyclic ranges and peaks, it is also possible to confirm Balazs' [34] approach to using the monotonic bond stress slip relationship as the failure envelope for bond under high-cycle fatigue. Also shown in Table 3 are the age and concrete strength at testing. Specimens C1 to C4 were cycled to failure, CF in Column 4, and Specimens C5 to C13 were cycled and then loaded to failure, LF in Column 4. The peak of the cyclic stress is listed in the column labelled τ_{pk} followed by the cyclic trough stress τ_{tr}. The peak and trough shear stresses are given as a proportion of the peak monotonic strength τ_{max} in the columns labelled P and T, and R is the total

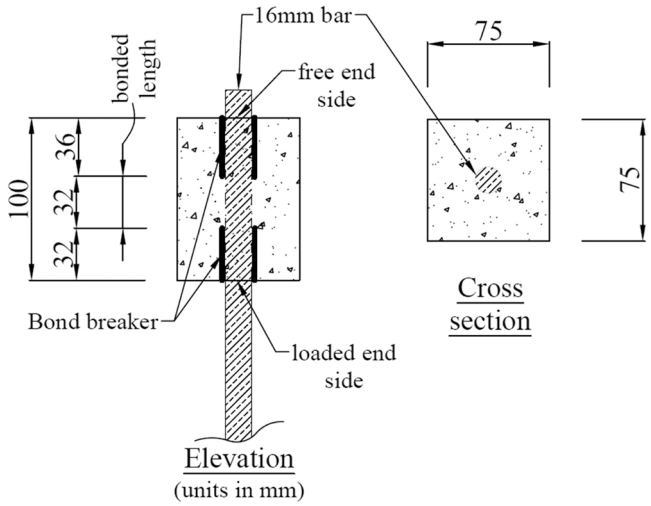

Fig. 2. Test specimen.

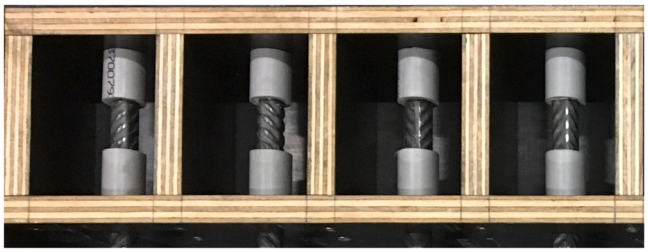

Fig. 3. Example of rib positions in specimens before casting.

Table 2
Concrete mix design.

Material	Mix ratio (by mass)
Sulphate resisting cement	1
Mined sand	1
Silica fume	0.266
Water	0.190
High-range water reducing agent with retarder	0.045
Steel micro fibres	0.163

Table 3
Fatigue tests.

Specimen Name	Age (days)	f_c (MPa)	Failure mode*	P (τ_{pk}/τ_{max})	T (τ_{tr}/τ_{max})	R (τ_r/τ_{max})	τ_{pk} (MPa)	τ_{tr} (MPa)
C1	50	115.3	CF	0.669	0.026	0.644	21.26	0.82
C2	33	110.8	CF	0.695	-0.195	0.890	22.08	-6.19
C3	117	129.9	CF	0.763	-0.046	0.809	24.22	-1.46
C4	49	115.0	CF	0.866	0.034	0.831	27.49	1.09
C5	36	111.6	LF	0.472	-0.139	0.611	15.00	-4.40
C6	118	130.1	LF	0.670	-0.053	0.722	21.27	-1.67
C7	51	115.5	LF	0.673	0.026	0.647	21.37	0.83
C8	83	123.9	LF	0.374	-0.058	0.432	11.87	-1.86
C9	110	128.8	LF	0.475	0.024	0.452	15.10	0.75
C10	75	121.8	LF	0.869	0.424	0.445	27.59	13.46
C11	90	125.7	LF	0.870	0.617	0.253	27.64	19.60
C12	103	127.7	LF	0.275	0.020	0.255	8.73	0.63
C13	96	126.6	LF	0.161	-0.057	0.218	5.10	-1.82

range as a proportion of τ_{max}.

The test rig is shown in Fig. 4(b) and schematically in Fig. 4(a), where the specimen is hatched. The concrete block is fully restrained by two plates such that all measured displacements were made relative to these plates. The plates are adjustable and tightened to hold the concrete block without applying undue compression. The free-end side of the specimen is located at Plate 2 where a single transducer was used to directly measure the reinforcement slip at the free-end. At the fixed-end, two transducers are fixed to the reinforcing bar as shown. The slip at the fixed-end is the deformation in the transducers less the rebar elongation due to the axial strain induced by the applied load between the fixed-end of the specimen and where the transducers are fixed.

The five monotonic tests were performed under displacement control. The tests were started at a constant displacement rate of 0.1 mm/min until the specimen reached a slip of 1 mm. The displacement rate was then increased to 0.5 mm/min and stopped at 20 mm, which was more than double the rib spacing, such that the only interface shear mechanism is pure friction, that is, no significant interface shear existed.

The thirteen specimens in Table 3 were tested under cyclic loading. The specimens were first monotonically loaded under displacement control at a rate of 0.25 mm/min until the required peak stress τ_{pk} was achieved, that is, point *a* in Fig. 1(a). The specimen was then unloaded at the same rate to τ_{tr}, then loaded to the mean of the peak and trough and then cycled under load control at a frequency (f) of 10 Hz for both the CF and LF tests.

3. Monotonic test results

All the tests, both the monotonic and cyclic, eventually failed by pull-out. Fig. 5(a) shows the concrete failure plane for a monotonically tested specimen and Fig. 5(b) for a specimen that was cycled to failure. The rib indents can be clearly seen in Fig. 5(a), and so too can the scratches they produced during pull-out failure. It can be seen that cyclic loading has caused the concrete adjacent to

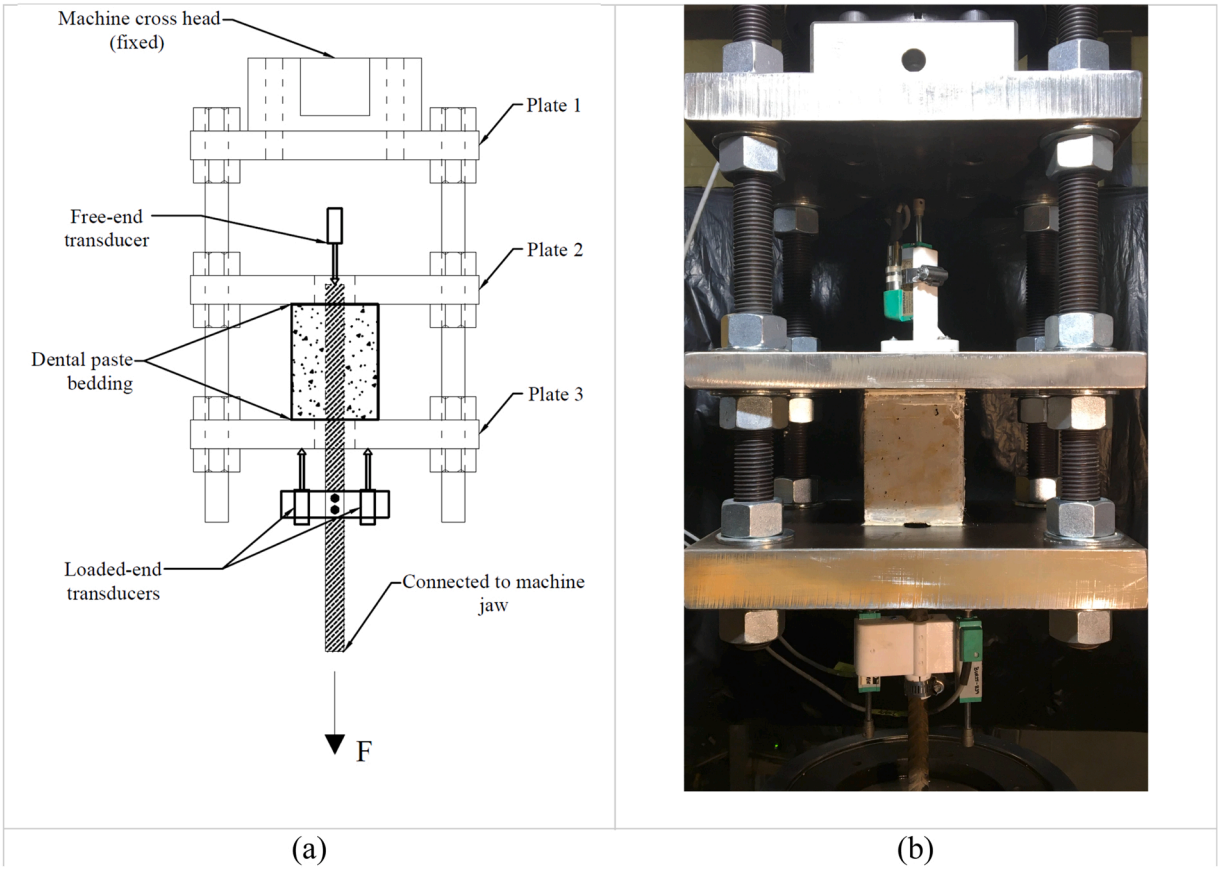

Fig. 4. Test rig: (a) Schematic representation; (b) Rig.

the bar impression in Fig. 5(a) to be removed by powdering as in Fig. 5(b).

The individual results for each test are given in Fig. S1 in the Supplementary Material, where it can be seen that there is a negligible difference between the slips at the free and fixed ends. The average of the free-end and loaded-end slips are plotted in Fig. 6. There would appear to be an ascending branch, followed by a ductile plateau and then a descending branch. This ductile plateau has been noted before by Li et al. [8], where it was felt that it was due to the fibres providing confinement to the concrete encasing the reinforcement. A similar effect is recognised by CEB-Fib Bulletin 10 [34], where confined concrete as through stirrups or fibres creates a bond-slip ductile plateau of the confined reinforcement.

The results of a regression analysis of the test data in Fig. 6 are given by Eqs. (5)–(7) and shown in Fig. 7. The dashed line in Fig. 7 is given with the upper and lower 5% confidence limits and which are compared with the average of the monotonic test results in Fig. 6.

The plateau at the peak stress τ_{max} occurs at 31.3 MPa and extends from the peak of the ascending branch at S_{asc} of 0.180 mm to S_{max} of 1.273 mm that is

$$\tau = 31.3 \text{ when } 0.180 < S < 1.273 \tag{5}$$

A non-linear fit to the ascending branch is given by

$$log_{10}S = 2.817 log_{10}\tau - 4.957 \text{when } S < \quad 0.18 \tag{6}$$

The descending branch can also be assumed linear, and the fit is given by

$$S = 12.80 - 0.368\tau \text{ when } S > 1.273 \tag{7}$$

where the units of Eqs. (5)–(7) are N and mm, and these properties are only applicable to the UHPFRC tested.

Eq. (6) can be used to determine S_{st} at point a in Fig. 1(a). Eq. (7) can be used to determine S_{po} at point *f,* and Eq. (5) can be used to determine the range of slip of the ductile plateau at τ_{max}.

4. Cyclic test results

Specimen C4 in Fig. 8 is a typical example of the bond-slip behaviour for a specimen cycled to failure. This specimen was first

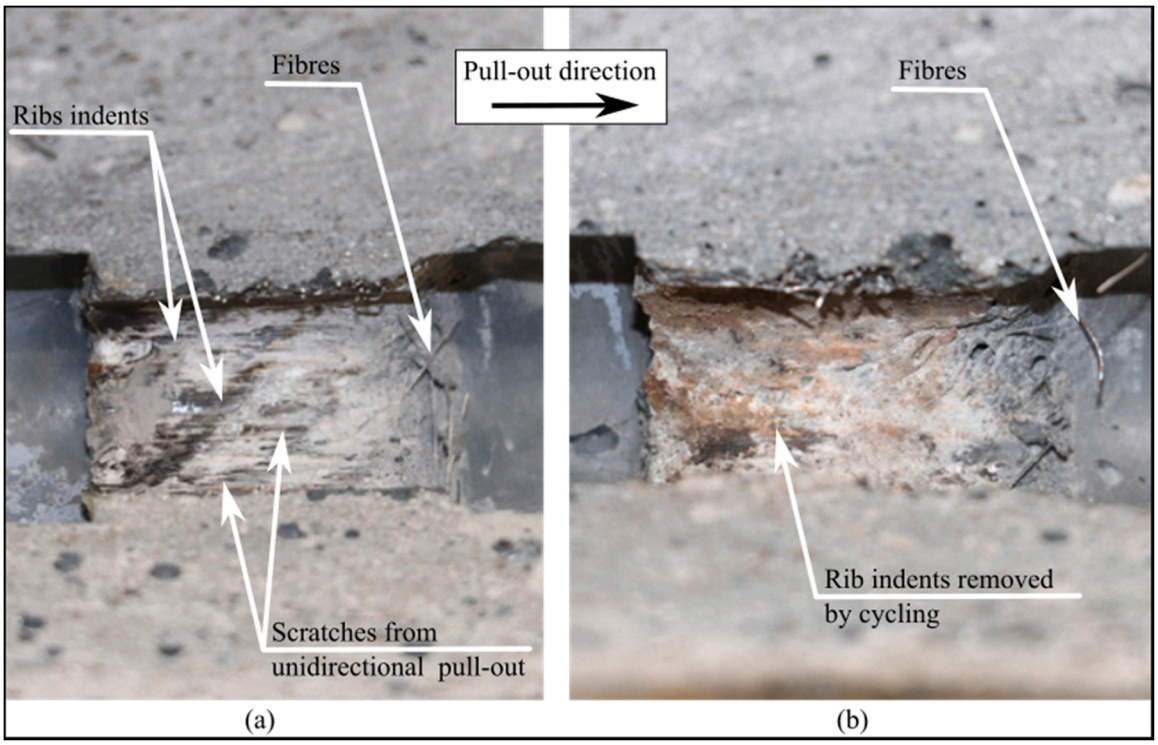

Fig. 5. Concrete bonded area after test: (a) Monotonic specimen (M5); (b) Cyclic specimen (C9).

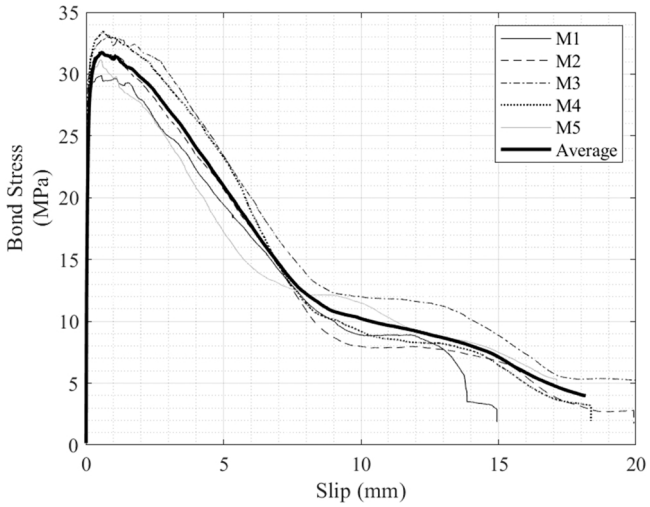

Fig. 6. Monotonic test results.

monotonically loaded to τ_{pk} of 27.49 MPa in Table 3, which is point *a* in Fig. 1 and then unloaded to τ_{tr} such that the required mean cyclic shear stress was obtained. The load was then cycled at 10 Hz until the peak stress could not be achieved and was limited by the monotonic envelope.

For later analysis, the point at which the peak stress could not be achieved was defined as when the peak stress reduced by 1% to give point *f*; this point is N_{po} and S_{po} in Fig. 1 and is listed in Table 4. All the CF test plots are given in Fig. S2 in the Supplementary Material. The slips S_{po} are plotted in Fig. 9, where it can be seen that they are in good agreement with the descending branch, particularly when the scatter of monotonic test results shown in Fig. 6 is considered. That is S_{po} in test C1 appears to fail at a load similar to that suggested by the least ductile monotonic test (M5).

Specimen C5 in Fig. 10 is typical of a specimen first cycled and then loaded to failure; all the bond-slip plots are given in Fig. S3 (a)

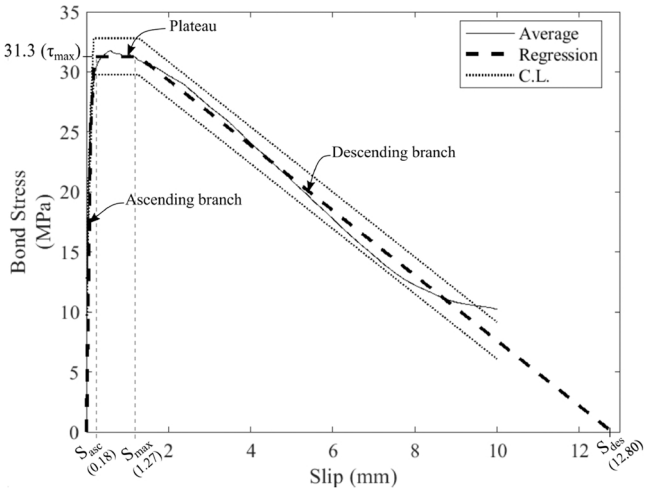

Fig. 7. Best fit of monotonic test results.

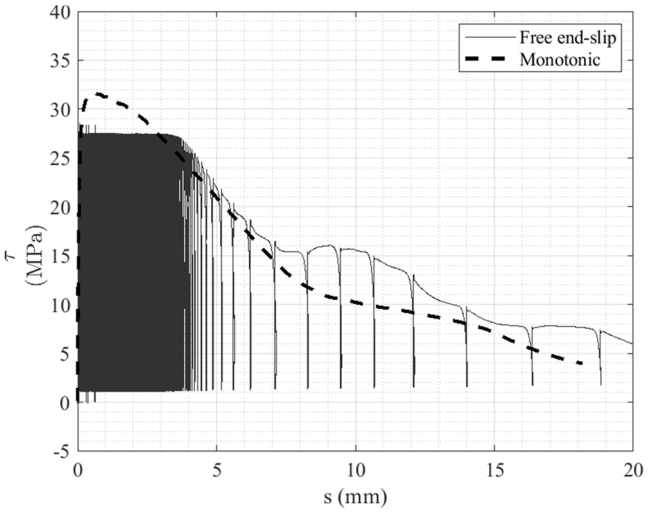

Fig. 8. Typical test cycled to failure (C4).

Table 4
Fatigue test results.

Specimen Name	τ_{rs} (MPa)	N_t	N_{tran}	N_{stb}	s_{max} (mm)	N_{po}	s_{po} (mm)	β_{tran}	β_{stb}	β_{unstb}
C1	–	88,492	2500	76,500	1.455	88,461	3.001	1.153E-04	1.495E-05	1.292E-04
C2	–	1,672,874	110,000	1,200,000	1.160	1,659,070	4.618	4.183E-06	5.802E-07	7.533E-06
C3	–	141,475	220	100,000	1.128	141,435	3.981	2.603E-04	9.850E-06	6.887E-05
C4	–	210,450	19,000	180,000	1.452	210,425	3.599	2.048E-05	5.826E-06	7.057E-05
C5	33.55	6,708,046	181,000	–	–	–	–	9.488E-07	4.587E-08	–
C6	36.95	5,106,974	155,000	–	–	–	–	2.692E-07	3.264E-08	–
C7	35.36	6,200,094	100,000	–	–	–	–	-1.199E-07*	3.074E-09	–
C8	34.56	6,000,148	500	–	–	–	–	5.304E-06	5.641E-10	–
C9	34.93	5,132,172	100000	–	–	–	–	1.209E-07	-1.441E-09*	–
C10	35.86	6,792,525	200,000	–	–	–	–	1.623E-07	2.021E-09	–
C11	34.31	4,916,448	30,000	–	–	–	–	8.790E-09	3.231E-09	–
C12	31.84	1,034,223	20,000	–	–	–	–	3.342E-06	9.185E-09	–
C13	34.84	5,145,178	500	–	–	–	–	6.269E-06	-1.568E-09*	–

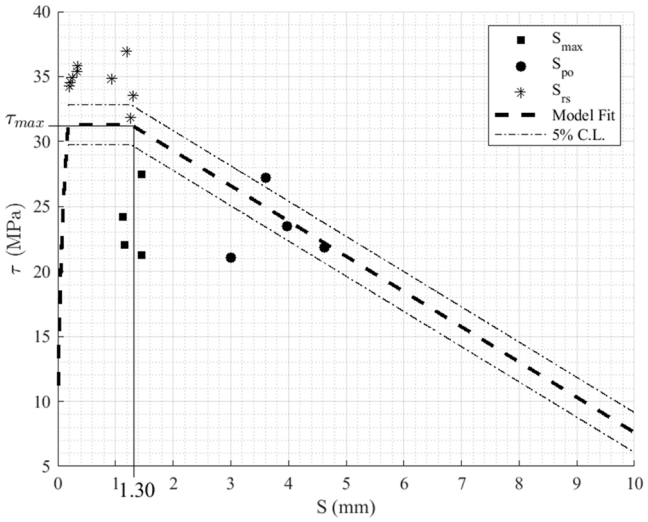

Fig. 9. Comparison of cyclic results with monotonic behaviour.

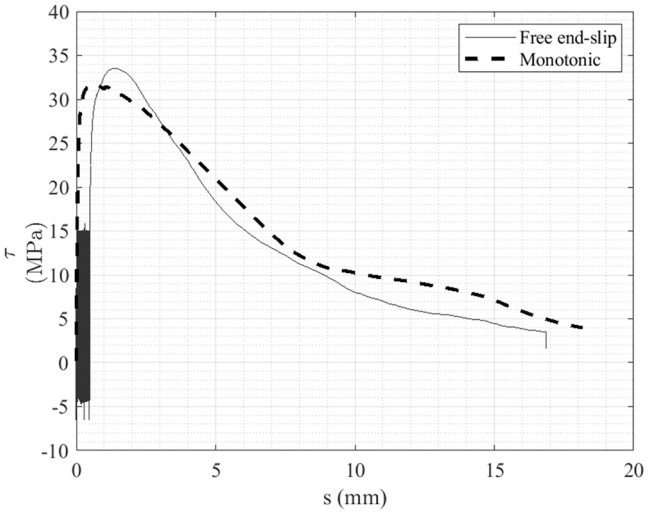

Fig. 10. Typical test loaded to failure (C5).

and (b) in the Supplementary Material. The residual strengths τ_{rs} are listed in Table 4 and plotted in Fig. 9, where it is interesting to note that they were 9% higher than the average $\tau_{max,}$ probably due to confinement provided by the fibres as micro-cracks form during the cyclic load history.

5. Analysis of incremental set data

For the UHPFRC used in the tests, the interaction Fig. 1 has been idealised to that in Fig. 11. The monotonic envelope has been drawn with an ascending branch which reaches τ_{max} at S_{asc} and continues at τ_{max} up to the slip of S_{max}. Hence, S_{max} is now defined as the slip at the end of the plateau, after which the stress reduces with increases in slip in a linear way. It will be shown in Section 7 on cyclic stiffness that the change in cyclic slip from the trough to the peak is about 0.03 mm, which is two orders of magnitude smaller than S_{max}. Hence the cyclic loads in Fig. 11(a) have been drawn as horizontal lines to emphasise that the cyclic slip at the trough or mean is virtually the same as that at the peak.

The incremental set chart shown in Fig. 1(b) and now shown in Fig. 11(b) can be divided into four regions: (1) the transition to a stable region (A-B) that is where the incremental set is first rapid, then stabilises to β_{stb} and which has an average value of β_{tran}; (2) the stable region (B-D) where the incremental set is constant at β_{stb}; (3) the unstable region (D-F) where the incremental set rapidly increases and which has an average value of β_{unstb}; and (4) the pull out region (F-G). It is a question of quantifying these regions. On first loading, the slip S_{pk} at the peak of the cyclic load can be derived from the ascending branch of the monotonic envelope from, for

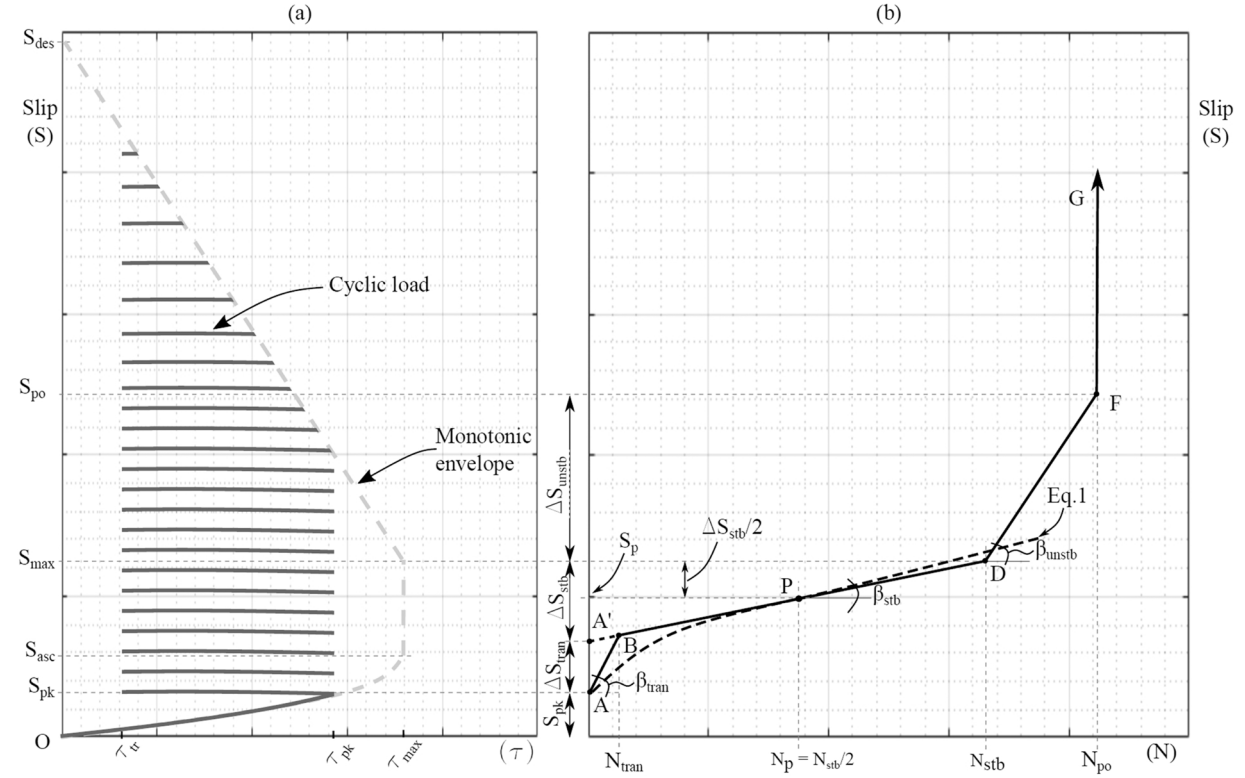

Fig. 11. Idealised interaction for UHPFRC.

example, Eq. (6), hence point A in Fig. 11(b) is known. Cyclic loading in the stable region can continue until the slip S_{max} is reached, which gives just one coordinate of point D. The remaining coordinates are quantified in the following subsections.

The incremental set chart for each test was constructed using the slip at the mean cyclic load for the descending branch of each cycle. Fig. 12 is typical of a specimen cycled to failure and Fig. 13 for those loaded to failure. All the tests are given in Fig. S4 in the Supplementary Material, which are grouped in their nominal ranges for comparison and the key points are listed in Table 4.

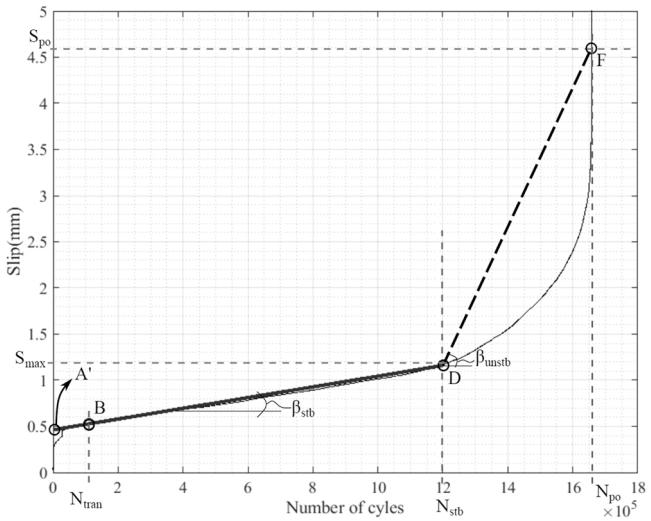

Fig. 12. Typical incremental set for specimen (C2) cycled to failure.

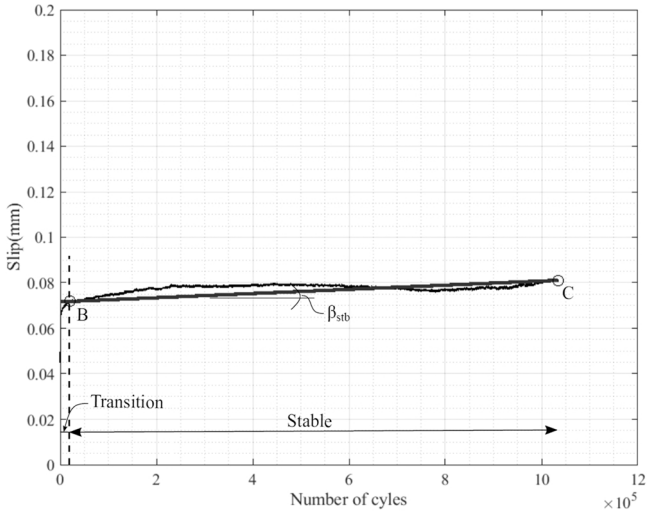

Fig. 13. Typical incremental set for specimen (C12) loaded to failure.

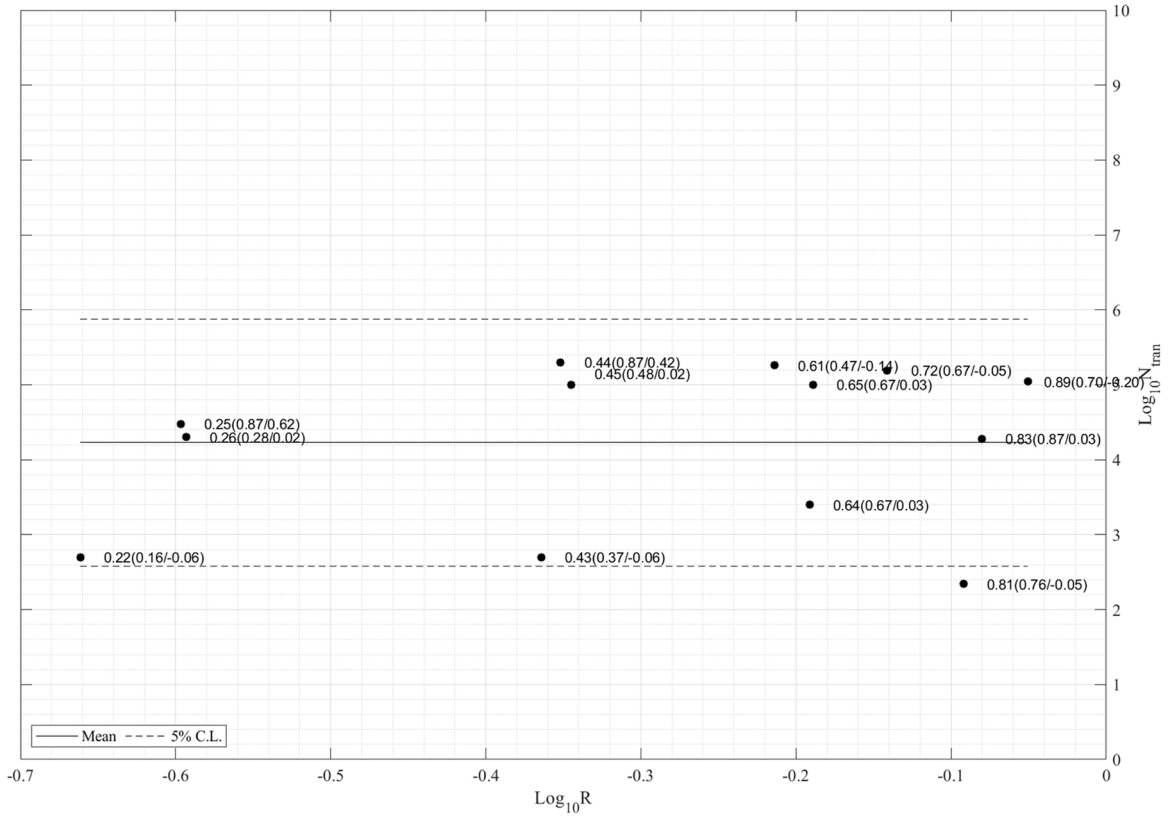

Fig. 14. Variation of N_{tran} with R.

5.1. Transition zone

Point A in the transition zone in Fig. 11(b) occurs at S_{pk}, which is known. Hence point B has to be fixed by quantifying both N_{tran} and β_{tran}. The number of cycles to stabilise the incremental set N_{tran} are listed in Table 4 and plotted against the total range R in Fig. 14, from which there would appear to be no correlation, and N_{tran} has a mean of

$$log_{10}N_{tran} = 4.230 \tag{8}$$

and a standard deviation of 1.079. Hence about 17 thousand cycles are required to stabilise the incremental set for the range of ranges used in these tests. Although the standard deviation is high, this is to be expected in fatigue testing and is similar in magnitude to that observed in other studies [28].

The values of β_{tran} from the experimental data are listed in Table 4 and plotted against R in Fig. 15, where a linear regression analysis gave

$$log_{10}(\beta_{tran}) = \quad -4.873 + 2.561 log_{10} R \tag{9}$$

and which has a standard deviation of

$$SD_{\beta tran} = 1.220 \tag{10}$$

Eqs. (9) and (10) can be written as

$$\beta_{tran} = \quad 1.340 \bullet 10^{-5} \bullet R^{2.561} \bullet 10^{\pm x SD_{\beta_{tran}}} \tag{11}$$

where x is the number of standard deviations for the required confidence limit.

The extension of D-B in Fig. 11(b) to intercept the ordinate is point A′, which is an effective slip from which β_{stb} can be used from zero to N_{stb} cycles. The increase in slip from A to A′ that is ΔS_{tran} is given by

$$\Delta S_{tran} = N_{tran}(tan\beta_{tran} - tan\beta_{stb}) \tag{12}$$

where, N_{tran} and β_{tran} can be obtained from Eqs. (8) and (11) and β_{stb} from the ensuing section.

5.2. Stable zone

Fig. 12 is a typical result of a specimen cycled to failure where B-D is the stable region and where the end of the stable region at point D occurs at N_{stb} at $S_{max,}$ and the slope is β_{stb}. All the specimens CF are shown in Fig. S5 in the Supplementary Material, where the stable regions are shown as dashed lined, and where their values of N_{stb}, S_{max} and β_{stb} are listed in Table 4. The four values of S_{max} in Table 4 are plotted as black squares in Fig. 9. It can be seen that they are in reasonably close agreement with the slip at the end of the τ_{max} plateau at 1.30 mm that was obtained from a regression analysis of the monotonic results, which confirms Balazs's [27]

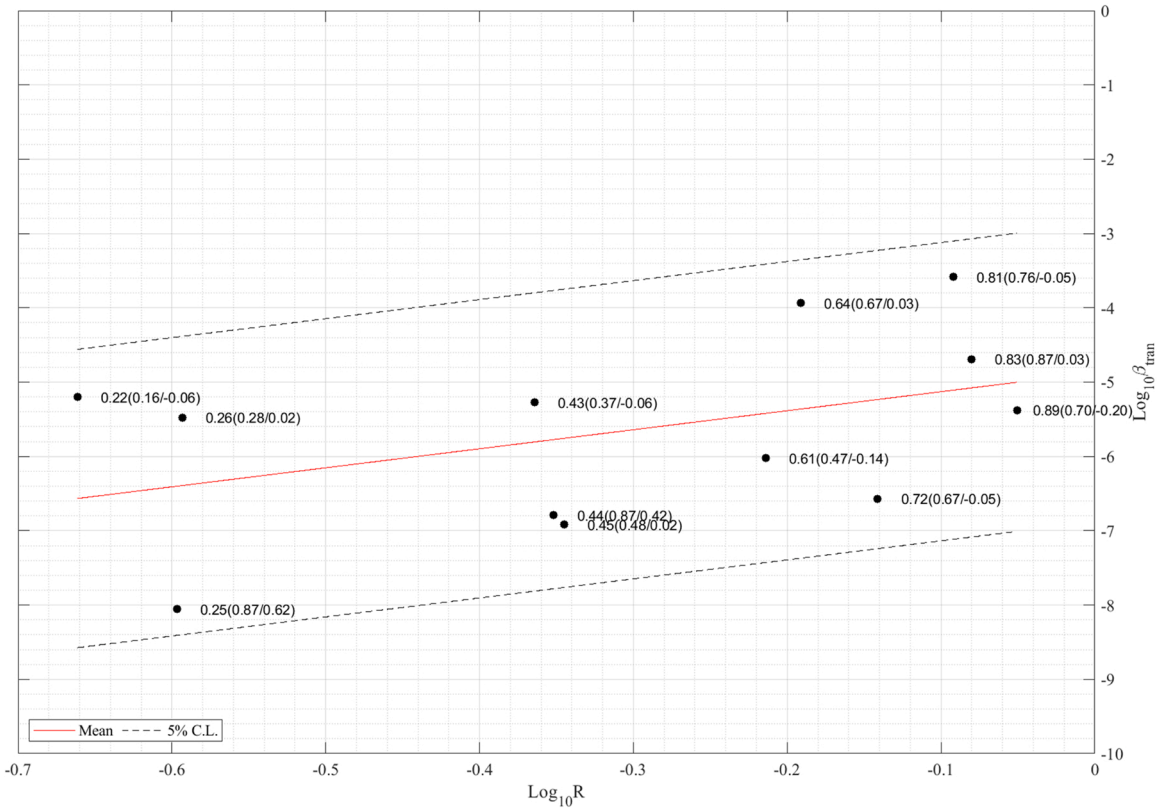

Fig. 15. Variation of β_{tran} with R.

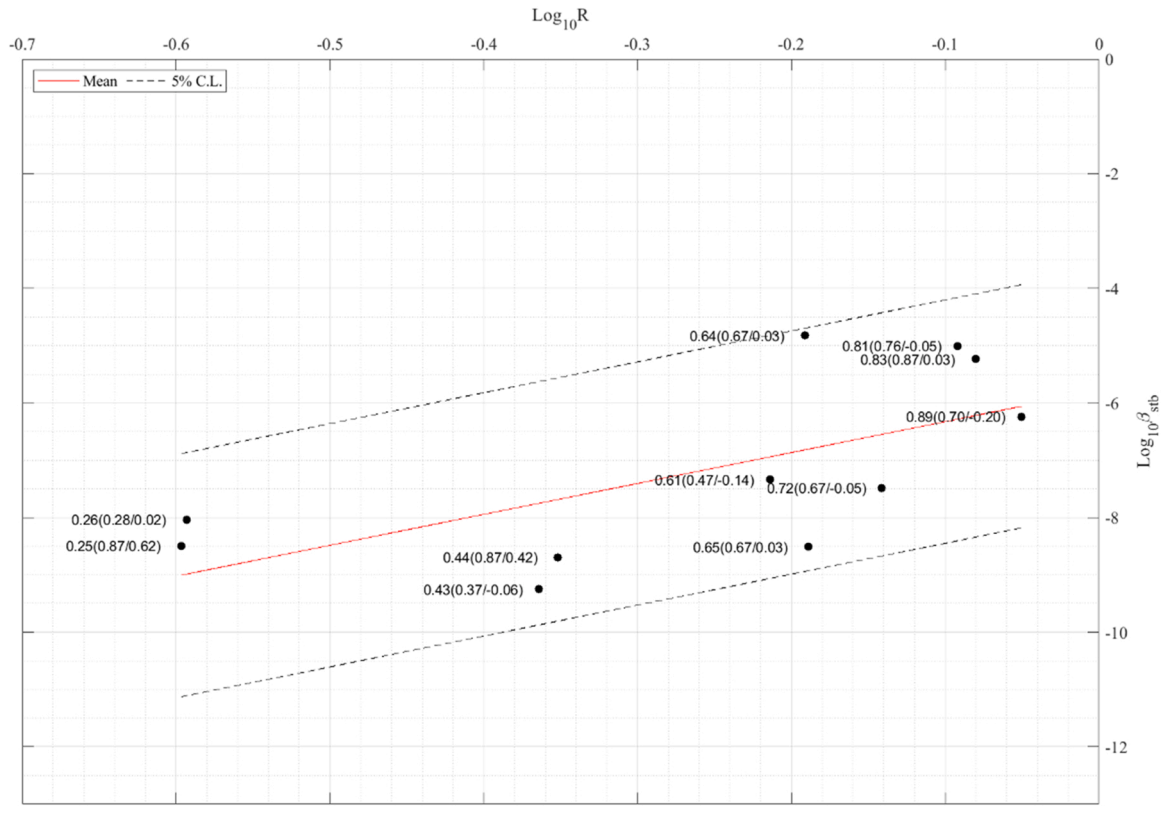

Fig. 16. Variation of β_{stb} with R.

conclusion for the extent of the stable region. Fig. 13 is typical of the specimens loaded to failure, and all of the LF specimens are shown in Fig. S6 in the Supplementary Material and their slopes β_{stb} listed in Table 4.

A regression analysis of β_{stb} in Table 4 against the total cyclic range R from Table 3 is shown in Fig. 16 and gives

$$log_{10}(\beta_{stb}) = \quad -5.787 + 5.394 log_{10} R \tag{13}$$

which has a standard deviation of

$$SD_{\beta_{stb}} = 1.290 \tag{14}$$

such that Eqs. (13) and (14) can be written as

$$\beta_{stb} = 1.633 \bullet 10^{-6} \bullet R^{5.394} \quad \bullet 10^{\pm x SD_{\beta_{stb}}} \tag{15}$$

The two specimens marked with an asterisk in Table 4 were omitted as they showed no fatigue damage, that is β_{stb} was negative, which will give a conservative value in design.

From Fig. 11, it can therefore be seen that fatigue failure occurs when

$$S_{pk} + \Delta S_{tran} + \Delta S_{stb} = S_{max} \tag{16}$$

Hence using the above approach all that is required to quantify fatigue failure has been determined.

5.3. Unstable zone

The four values of the slip at pullout failure S_{po} in Table 4 are plotted as black circles in Fig. 9 and show good correlation with the descending branch. This confirms that pullout occurs at point *f* in Fig. 1 that is when the increasing slip due to cyclic loading at the peak cyclic stress reaches the monotonic envelope given by Eq. (7).

The four values for β_{unstb} in Table 4 showed no correlation with R. They had a mean of

$$log_{10}\beta_{unstb} = \quad -4.331 \tag{17}$$

with a standard deviation of

$$SD_{\beta_{unstb}} = 0.543 \tag{18}$$

Fatigue design will probably be based on N_{stb} as the shear strength τ_{max} at N_{stb} has not yet reduced. Hence Eq. (17) will not be needed for fatigue design. However, Eq. (17) can be used to give an assessment of the remaining life and strength should N_{stb} be exceeded as will be explained in the following section on the accumulated used life.

5.4. Cyclic increase in slip

From Eqs. (14) and (15), the increase in slip in the stable region ΔS_{stb} in Figs. 1(b) and 11(b) for a given number of cycles N_{blk} is given by

$$\Delta S_{stb} = N_{blk} \bullet 1.633 \bullet 10^{-6} \bullet R^{5.394} \quad \bullet 10^{\pm xSD_{\beta_{stb}}} \tag{19}$$

For the unstable region and using Eqs. (17) and (18), the increase in slip is given by

$$\Delta S_{unstb} = N_{blk}\left(46.67 \bullet 10^{-6} \bullet 10^{\pm 0.543x}\right) \tag{20}$$

6. Accumulated used-life of specimens

An accumulated damage law will be derived for a range of stresses on the test specimen in Fig. 2. These specimens were specifically designed to have a uniform slip and consequently a uniform interface shear stress in order to extract the fatigue properties. Let us assume that a specimen is subjected to z cyclic ranges, as shown in Column 1 in Table 5. The frequency at which these ranges of stress occur is listed in Column 2; for convenience of explanation, let us assume that these are the frequencies, that is the number of cycles, over one full year. It has been shown in the above research that the bond strength τ_{max} does not reduce during the stable region in Fig. 1 (b) and that it reduces in the unstable region. Let us first consider the stable region.

6.1. Fatigue assessment in stable region

Each individual cycle of stress causes an increase in bond slip of β_{stb}. Therefore, the full spectrum of ranges of stress in Table 5, where the incremental set for each range is given in Column 3, causes the following increase in slip over a time period of one full year

$$\Delta S_{stb-fat} = \sum_{k=1}^{k=z} \beta_{stb-k} f_k \tag{21}$$

which can be derived from Eq. (19) and can be referred to as the fatigue damage.

The bound between the stable and unstable regions occurs at a slip of S_{max} as shown in Fig. 11(b). Therefore, the maximum allowable slip due to cyclic loading within the stable region is given by

$$\Delta S_{stb} = S_{max} - S_{pk} - \Delta S_{tran} \tag{22}$$

In fatigue analyses [35], the fatigue damage D is often defined as the actual damage as a proportion of the allowable damage, which from Eqs. (21) and (22) is

$$D_{stb} = \sum_{k=1}^{k=z} \frac{\beta_{stb-k} f_k}{S_{max} - S_{pk} - \Delta S_{tran}} \tag{23}$$

When the numerator is smaller than the denominator in Eq. (23), the component is still within its stable region and the strength has not reduced. Furthermore, as the force spectrum in Table 5 is over one full year, then the inverse of the fatigue damage, that is $1/D_{stb}$, is the fatigue life of the component in years and which is the fatigue life in which there is no reduction in the bond strength.

It can be seen in Eq. (23) that two very important fatigue material properties govern the fatigue damage, that is the incremental set β and the slip S_{max} at the end of the τ_{max} plateau in Fig. 7. It is also of importance to realise that this fatigue damage equation is specifically based on slips and not an accumulation of empirically derived endurances as is the case with most endurance equations for other types of components. Although it would be difficult to use this equation in the assessment of RC structures as they are subjected to varying bond stresses [36–38], it is important to note that the equation does show that when a crack width exceeds $2S_{max}$ then the design fatigue life at that point is exceeded. Hence, monitoring the crack widths in a structure subjected to fatigue loads would be a

Table 5
Fatigue assessment.

Range (R)	Frequency (f)	β_{stb}	β_{unstb}
R_1	f_1	$\beta_{stb\text{-}1}$	$\beta_{unstb\text{-}1}$
R_2	f_2	$\beta_{stb\text{-}2}$	$\beta_{unstb\text{-}2}$
–	–	–	–
R_z	f_z	$\beta_{stb\text{-}z}$	$\beta_{unstb\text{-}z}$

useful approach in checking for fatigue damage.

6.2. Fatigue assessment in unstable region

The above approach can be applied to the unstable region in Figs. 1(b) and 11(b) to give

$$D_{unstb} = \sum_{k=1}^{k=z} \frac{\beta_{unstb-k} f_k}{S_{po} - S_{max}} \tag{24}$$

where S_{po} is the monotonic slip at the maximum peak cyclic stress τ_{pk} as in Fig. 1(a) and which can be calculated with the help of Eq. (7).

The inverse of D_{unstb} in Eq. (24) is the number of years within the unstable region (that is, after the stable region years) during which the bond shear strength has reduced from τ_{max} to τ_{po}. However, Eq. (24) can also be used to derive the design life prior to pull out, such as at point h in Fig. 1(a), in which case S_{po} would be substituted with S_{rs}. It can now be seen the importance of the monotonic descending branch in Fig. 7 in allowing for assessment of the bond strength at the crack width of $2S_{rs}$.

7. Cyclic stiffness

The cyclic stiffness k is defined in Fig. 1(a) as the range of stress τ_r divided by the slip in the half cycle. An example of the variation in Specimen C2 is shown in Fig. 17, where much of the scatter is due to the difficulty in measuring the very small slips in a cycle. To minimise the scatter, linear regression analyses were performed in the stable and unstable regions separately. Importantly, the cyclic stiffness is seen to be larger in the unstable region than in the stable region, but this increase in stiffness occurs because the stress range is reduced in the unstable region because the peak stress is limited by the monotonic envelope (see Fig. 1). These regression analyses were then used to determine the cyclic stiffnesses at the start of cyclic loading k_{st} at point A in Fig. 11, at the transition point k_{stb} at point D and at the onset of pullout k_{po} at point F.

All the k_{st} values are plotted in Fig. 18. It can be seen that the cyclic stiffness at the start reduces slightly with increasing range and is given by

$$k_{st} = 1009R^{-1.603} \tag{25}$$

and which has a standard deviation of 0.340 and where the units are in N and mm.

A similar analysis at the transition point D, in Figs. 1(d) and 11(b), gave

$$k_{stb} = 1276R^{-1.441} \tag{26}$$

which had a standard deviation of 0.367. There was no correlation between k_{po} and R which had a mean stiff of

$$k_{po} = 1723 \tag{27}$$

and a standard deviation of

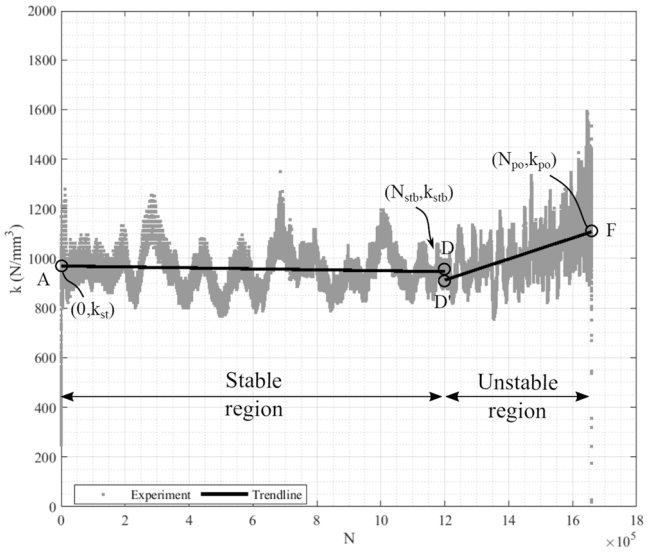

Fig. 17. Typical variation of cyclic stiffness (C2).

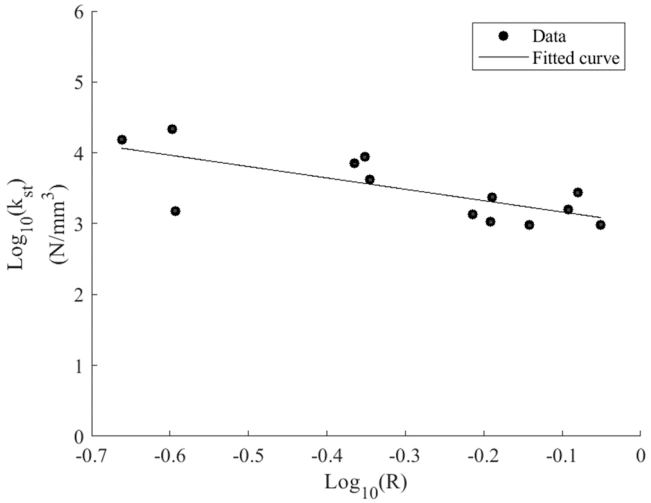

Fig. 18. Cyclic stiffness at the start of cyclic loading.

$$SD_{kpo} = 0.224 \tag{28}$$

8. Comparison with published approaches

As explained previously, Eq. (1) has been previously used to quantify the increase in slip due to cyclic loading using a range of b values listed in Table 1. Eq. (1) has only two variables that is the initial slip S_{st} and the exponent b, as compared with the approach developed in this paper, which quantifies the slip through the interaction between the cyclic and monotonic behaviours.

Eq. (1) is illustrated in Fig. 11 where the initial slip at point A, that is S_{st} in Eq. (1), is S_{pk} and, therefore, the only unknown factor is the exponent b. The two approaches have been compared at point P in Fig. 11 where N_p is half $N_{stb}/2$ and S_p is half way along ΔS_{stb}. In terms of these variables, Eq. (1) can be rearranged as

$$b = \frac{log_{10}S_p - log_{10}S_{pk}}{log_{10}(1+N_p)} \tag{29}$$

The exponent b was determined for each of the 13 cyclic specimens in Table 3, and a multivariable linear regression analysis of b values against their R and P values gave

$$b = 0.361 - 0.259P + 0.0804R \tag{30}$$

that had a very high R^2 of 0.967, which emphasises the importance of both R and P and subsequently the interaction between the monotonic and cyclic behaviours.

Given that each of the models described in Table 1 and developed here have been calibrated on a specific dataset, it is not possible to compare directly to test results. As an alternative, here the models are compared to each other by considering several different combinations of cyclic range and peak. The outcomes of this comparison are shown in Fig. 19, where the models in Table 1 are compared to the model proposed in Section 5, and also based on the recalibration of Eq. (1) with the b parameter given by Eq. (30).

In the comparison presented in Fig. 19, a slip at failure S_{max} of 1.27 mm was applied such that the number of cycles (N) to cause bond failure can be found for any combination of cyclic range and peak.

As described in Section 1, existing approaches have been calibrated on the basis that behaviour is influenced by cyclic peak but not for the range variation, and so in Fig. 19a-c, results are plotted for a constant range and varying peak (20%τ_{max}, 60% τ_{max} and 80% τ_{max}). The outcome of this comparison shows that the slip and the number of cycles to fail a specimen varies significantly for each peak load depending on the model chosen. For example, the estimated number of cycles for a peak equal to 20% reached up to 10^{29} cycles, while for 80% of the peak bond stress (τ_{max}), the number of cycles considered to cause fail was 10^{12}.

As it was shown in this work that both the cyclic range and peak impact the fatigue endurance, in Fig. 19d-f results are shown for 20%, 60% and 80% range with a 40% cyclic. Importantly, while it can be seen that for the existing models the predicted endurance does not change, for the models proposed here, the endurance is significantly impacted.

By comparing the two approaches proposed in this work, it can be observed in Fig. 19 that the simplified model (Eq. (30)) is a conservative approximation of the model developed in Section 5 and predicts significantly larger slips at lower numbers of cycles.

When considering all models, it is worth mentioning that calibration has been performed using data from tests that have

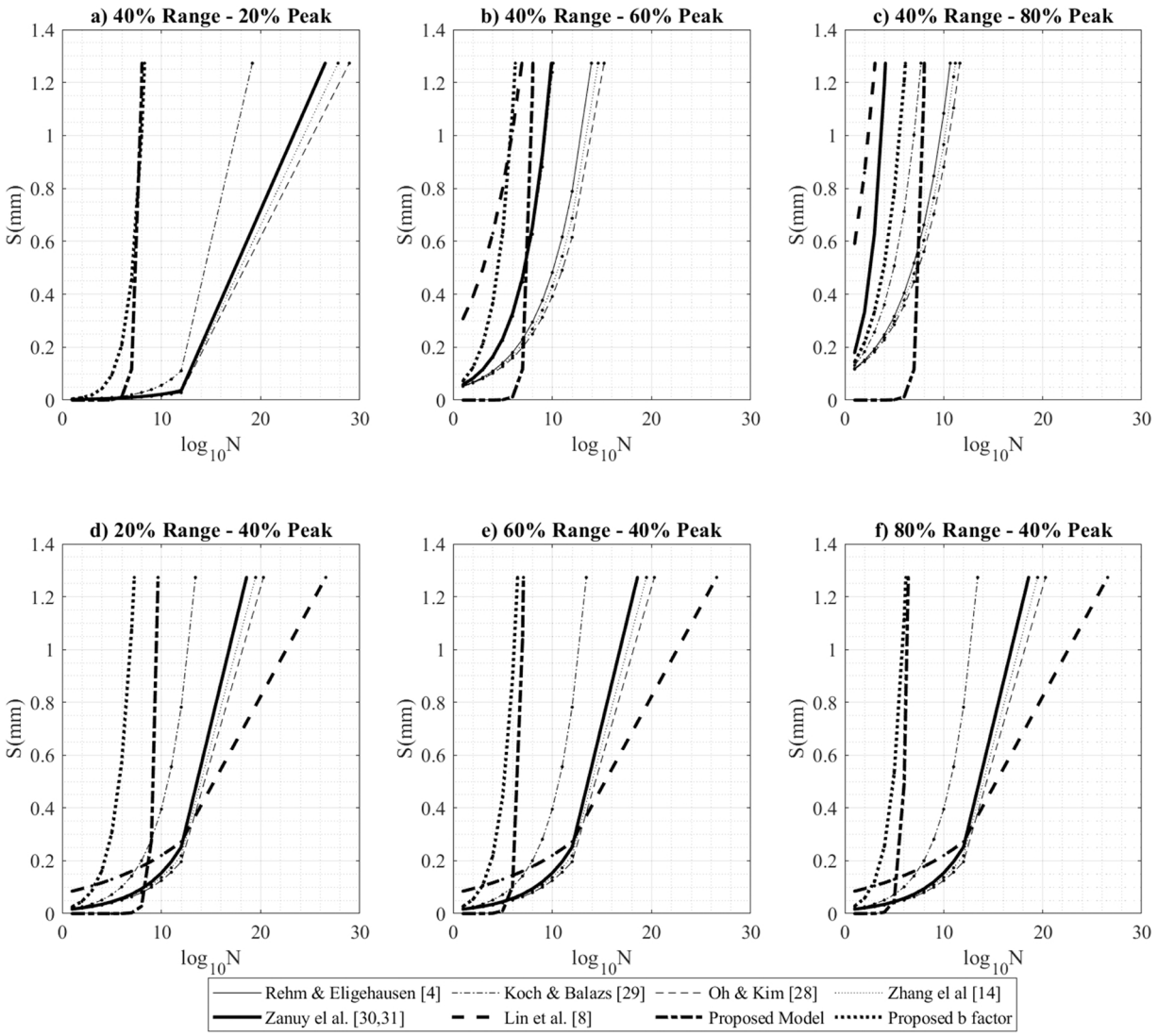

Fig. 19. Comparison of proposed model and proposed b factor with others equations.

predominately run out rather than have been cycled to failure and so further testing is required to validate models, particularly given the significant scatter in endurance in Fig. 19.

9. Conclusion

A testing and analysis procedure have been developed to quantify the fatigue properties of the bond-slip of steel reinforcing bars embedded in UHPFRC. It was found that the monotonic bond-slip properties were a very good envelope to the cyclic behaviours. Hence the monotonic envelope can be used to determine: the limit to the slip prior to which the bond shear strength did not reduce; and beyond this limit the reduction in the shear strength due to cyclic loading, and the slip at pullout.

Four distinct fatigue material zones were identified under cyclic loading. The initial transition zone during which the incremental set, that is the increase in slip per cycle, stabilised, the zone in which the incremental set was stable, followed by the unstable region in which the incremental set increased leading to the fourth pullout zone. The range of the cyclic load controlled the rate of the incremental set, whereas the peak of the cyclic load controlled the extent of slip prior to pullout.

An accumulated damage law was developed to accommodate any range and frequency of cyclic loads. It was shown that this accumulated damage law was directly related by mechanics to the bond slip and could be used to assess the fatigue life during which the bond strength did not reduce, and the reduction in strength should the fatigue life be exceeded. Because the accumulated damage law was directly related to the bond-slip through mechanics, it was shown that a simple measurement of a crack width in an RC structure could be used to assess the remaining fatigue life as well as any deterioration in bond strength.

Finally, when comparing to existing approaches, it is shown that both the cyclic range and peak are important in defining the fatigue life, not just the peak as has previously been suggested.

Declaration of Competing Interest

The authors declare the following financial interests/personal relationships which may be considered as potential competing interests: Phillip Visintin reports financial support was provided by Australian Research Council. Deric Oehlers reports financial support was provided by Australian Research Council.

Data Availability

Data will be made available on request. All data, models, and code generated or used during the study appear in the submitted article.

Acknowledgement

This material is based upon work supported by the Australian Research Council Discovery Project 190102650.

Appendix A. Supplementary material

Supplementary data associated with this article can be found in the online version at doi:10.1016/j.cscm.2022.e01370.

References

[1] P. Visintin, D.J. Oehlers, C. Wu, M.C. Griffit, The reinforcement contribution to the cyclic behaviour of reinforced concrete beam hinges, Earthq. Eng. Struct. Dyn. 41 (2012) 1591–1608, https://doi.org/10.1002/eqe.1189.
[2] J. Cairns, Bond and anchorage of embedded steel reinforcement in fib Model Code 2010, Struct. Concr. 16 (2015) 45–55, https://doi.org/10.1002/suco.201400043.
[3] G.L. Balazs, Cracking analysis based on slip and bond stresses, Acids Mater. J. 90 (1993) 340–348.
[4] G. Rehm, R. Eligehausen, Bond of ribbed bars under high cycle repeated loads, Acids J. 76 (1979) 297–309.
[5] H. Lin, Y. Zhao, P. Feng, H. Ye, J. Ozbolt, C. Jiang, J.Q. Yang, State-of-the-art review on the bond properties of corroded reinforcing steel bar, Constr. Build. Mater. 213 (2019) 216–233, https://doi.org/10.1016/j.conbuildmat.2019.04.077.
[6] C. Zanuy, L. Albajar, P. De Fuente, Structural Effects of Bond Damage Due to Highly Repeated Loading, 2012, pp. 655–660.
[7] C. Fernandes, H. Varum, A. Costa, Importance of the bond-slip mechanism in the numerical simulation of the cyclic response of RC elements with plain reinforcing bars, Eng. Struct. 56 (2013) 396–406, https://doi.org/10.1016/j.engstruct.2013.05.013.
[8] H. Lin, Y. Zhao, J. Ožbolt, R. Hans-Wolf, The bond behavior between concrete and corroded steel bar under repeated loading, Eng. Struct. 140 (2017) 390–405, https://doi.org/10.1016/j.engstruct.2017.02.067.
[9] T.T. Akbas, O.C. Celik, C. Yalcin, A. Ilki, Monotonic and cyclic bond behavior of deformed CFRP bars in high strength concrete, Polymers 8 (2016), https://doi.org/10.3390/polym8060211.
[10] M. Deng, J. Pan, H. Sun, Bond behavior of deformed bar embedded in engineered cementitious composites under cyclic loading, Constr. Build. Mater. 197 (2019) 164–174, https://doi.org/10.1016/j.conbuildmat.2018.11.200.
[11] V.C. Li, T. Matsumoto, Fatigue crack growth analysis of fiber reinforced concrete with effect of interfacial bond degradation, Cem. Concr. Compos. 20 (1998) 339–351, https://doi.org/10.1016/S0958-9465(98)00010-9.
[12] A.K. Panda, R.A. Spencer, S. Mindess, Bond of deformed bars in steel fibre reinforced concrete under cyclic loading, Int. J. Cem. Compos. Light. Concr. 8 (1986) 239–249, https://doi.org/10.1016/0262-5075(86)90051-5.
[13] J. Seo, G.C. Lee, Z. Liang, G.F. Dargush, Configuration and size effects on bond stress-slip and failure modes of RC connections, J. Eng. Mech. 140 (2014), https://doi.org/10.1061/(ASCE)EM.1943-7889.0000790.
[14] W. Zhang, Y. Zhang, H. Li, X. Gu, Experimental investigation of fatigue bond behavior between deformed steel bar and concrete, Cem. Concr. Compos. 108 (2020), 103515, https://doi.org/10.1016/j.cemconcomp.2020.103515.
[15] R. Zou, F. Liu, Z. Xiong, S. He, L. Li, W. Wei, Experimental study on fatigue bond behaviour between basalt fibre-reinforced polymer bars and recycled aggregate concrete, Constr. Build. Mater. 270 (2021), 121399, https://doi.org/10.1016/j.conbuildmat.2020.121399.
[16] R. Eligehausen, V. Ciampi, V. Bertero, E. Popov. Analytical Model for Deformed Bar Bond under Generalised Excitations, 1981, https://doi.org/10.18419/opus-7970.
[17] L. Guizani, O. Chaallal, An experimental study on bond-slip in moderately confined concrete subjected to monotonic and cyclic loading using an experimental plan, Can. J. Civ. Eng. 38 (2011) 272–282, https://doi.org/10.1139/L10-133.
[18] M.H. Harajli, Bond behavior in steel fiber-reinforced concrete zones under static and cyclic loading: experimental evaluations and analytical modeling, J. Mater. Civ. Eng. 22 (2010) 674–686, https://doi.org/10.1061/(asce)mt.1943-5533.0000067.
[19] X. Hu, G. Peng, D. Niu, J. Wang, Bond properties of deformed steel bars in concrete during construction under reversed cyclic loading, Constr. Build. Mater. 223 (2019) 817–829, https://doi.org/10.1016/j.conbuildmat.2019.06.222.
[20] L. Huang, Y. Chi, L. Xu, P. Chen, A. Zhang, Local bond performance of rebar embedded in steel-polypropylene hybrid fiber reinforced concrete under monotonic and cyclic loading, Constr. Build. Mater. 103 (2016) 77–92, https://doi.org/10.1016/j.conbuildmat.2015.11.040.
[21] B. Kim, J.Y. Lee, Resistance of interfacial debonding failure of GFRP bars embedded in concrete reinforced with structural fibers under cycling loads, Compos. Part B Eng. 156 (2019) 201–211, https://doi.org/10.1016/j.compositesb.2018.08.091.
[22] L. Higgins, J.P. Forth, A. Neville, R. Jones, T. Hodgson, Behaviour of cracked reinforced concrete beams under repeated and sustained load types, Eng. Struct. 56 (2013) 457–465, https://doi.org/10.1016/j.engstruct.2013.05.034.
[23] J. Li, X. Gao, P. Zhang, Experimental investigation on the bond of reinforcing bars in high performance concrete under cyclic loading, Mater. Struct. Constr. 40 (2007) 1027–1044, https://doi.org/10.1617/s11527-006-9201-1.
[24] J. Yuan, B.A. Graybeal. Bond Behavior of Reinforcing Steel in Ultra-High Performance Concrete, 2014, https://doi.org/10.1159/000331754.

[25] A.B. Sturm, P. Visintin, Local bond slip behavior of steel reinforcing bars embedded in ultra high performance fibre reinforced concrete, Struct. Concr. 20 (2019) 108–122, https://doi.org/10.1002/suco.201700149.
[26] M. Koschemann, T. Kuhn, K. Speck, M. Curbach, Bond behaviour of reinforced concrete under high cycle fatigue pull-out loading, in: Better, Smarter, Stronger Proccedings 2018 Fib Congress, 2018.
[27] G. Balazs, Deformation based fatigue failure criterion, Eng. Sci. 4 (1994) 8.
[28] R. Koch, G.L. Balázs, Slip increase under cyclic and long term loads, Otto-Graf. J. Res. Test. Mater. Res. Test. Mater. 4 (1993) 160–191.
[29] B.H. Oh, S.H. Kim, Realistic models for local bond stress-slip of reinforced concrete under repeated loading, J. Struct. Eng. 133 (2007) 216–224, https://doi.org/10.1061/(asce)0733-9445(2007)133:2(216).
[30] C. Zanuy, P. de la Fuente, L. Albajar, Estimation of parameters defining negative tension stiffening, Eng. Struct. 32 (2010) 3355–3362, https://doi.org/10.1016/J.ENGSTRUCT.2010.07.009.
[31] C. Zanuy, I.M. Díaz, Stress distribution and resistance of lap splices under fatigue loading, Eng. Struct. 175 (2018) 700–710, https://doi.org/10.1016/J.ENGSTRUCT.2018.08.067.
[32] Australia/New Zeland Standard, AS/NZS 4671:2019 Steel for the Reinforcement of Concrete, 2019, p. 59.
[33] B.D.G. Sepulveda, P. Visintin, D.J. Oehlers, Quantifying the fatigue material properties of UHPFRC with steel microfibers at cracks, J. Struct. Eng. 147 (2021) 1–17, https://doi.org/10.1061/(asce)st.1943-541x.0003051.
[34] CEB-Fib, State-of Art-Report: Bond of Reinforcement in Concrete – Bulletin 10, 2000.
[35] D.J. Oehlers, M.A. Bradford. Composite Steel and Concrete Structural Members: Fundamental Behaviour, first ed., Pergamon, 1995.
[36] A.B. Sturm, P. Visintin, D.J. Oehlers, R. Seracino, Time-dependent tension-stiffening mechanics of fiber-reinforced and ultra-high-performance fiber-reinforced concrete, J. Struct. Eng. 144 (2018) 04018122, https://doi.org/10.1061/(asce)st.1943-541x.0002107.
[37] P. Visintin, D.J. Oehlers, R. Muhamad, C. Wu, Partial-interaction short term serviceability deflection of RC beams, Eng. Struct. 56 (2013) 993–1006, https://doi.org/10.1016/j.engstruct.2013.06.021.
[38] P. Visintin, A.B. Sturm, D.J. Oehlers, Long-and short-term serviceability behavior of reinforced concrete beams: mechanics models for deflections and crack widths, Struct. Concr. 19 (2018) 489–507, https://doi.org/10.1002/suco.201700022.